Nonequilibrium viscosity of glass

John C. Mauro, Douglas C. Allan, and Marcel Potuzak
Science and Technology Division, Corning Incorporated, Corning, New York 14831, USA
(Received 27 May 2009; revised manuscript received 24 August 2009; published 30 September 2009)

Since glass is a nonequilibrium material, its properties depend on both composition and thermal history. While most prior studies have focused on equilibrium liquid viscosity, an accurate description of nonequilibrium viscosity is essential for understanding the low temperature dynamics of glass. Departure from equilibrium occurs as a glass-forming system is cooled through the glass transition range. The glass transition involves a continuous breakdown of ergodicity as the system gradually becomes trapped in a subset of the available configurational phase space. At very low temperatures a glass is perfectly nonergodic (or "isostructural"), and the viscosity is described well by an Arrhenius form. However, the behavior of viscosity during the glass transition range itself is not yet understood. In this paper, we address the problem of glass viscosity using the enthalpy landscape model of Mauro and Loucks [Phys. Rev. B **76**, 174202 (2007)] for selenium, an elemental glass former. To study a wide range of thermal histories, we compute nonequilibrium viscosity with cooling rates from 10^{-12} to 10^{12} K/s. Based on these detailed landscape calculations, we propose a simplified phenomenological model capturing the essential physics of glass viscosity. The phenomenological model incorporates an ergodicity parameter that accounts for the continuous breakdown of ergodicity at the glass transition. We show a direct relationship between the nonequilibrium viscosity parameters and the fragility of the supercooled liquid. The nonequilibrium viscosity model is validated against experimental measurements of Corning EAGLE XG™ glass. The measurements are performed using a specially designed beam-bending apparatus capable of accurate nonequilibrium viscosity measurements up to 10^{16} Pa s. Using a common set of parameters, the phenomenological model provides an accurate description of EAGLE XG™ viscosity over the full range of measured temperatures and fictive temperatures.

DOI: 10.1103/PhysRevB.80.094204 PACS number(s): 61.43.Fs, 66.20.Cy, 66.20.Ej, 61.20.Lc

I. INTRODUCTION

A popular urban legend concerns the apparent flow of stained glass windows in medieval cathedrals. Since the stained glass pieces are often thicker at the bottom than at the top, many have surmised that the glass flowed slowly throughout the lifetime of the cathedral under the influence of gravity. A decade ago, this legend caught the interest of Zanotto,[1] who measured the shear viscosity (η) of several compositions commonly used in these windows. Due to experimental time constraints the viscosity could be measured only at elevated temperatures above the glass transition, i.e., in the supercooled liquid regime. Zanotto fitted these viscosity data to the empirical Vogel-Fulcher-Tammann (VFT) formula,[2–4]

$$\log_{10}\ \eta(T) = \log_{10}\ \eta_\infty + \frac{A_0}{T - T_0}, \tag{1}$$

where T is temperature and η_∞, A_0, and T_0 are fitting parameters. Extrapolating Eq. (1) to room temperature, Zanotto[1] estimated a relaxation time of about 10^{32} years, concluding that the stained glass could not have flowed during the lifetime of the cathedrals. Instead, the thickness variation could more likely be attributed to medieval glass processing techniques, which could not ensure a uniform thickness of the glass. When arranged in a stained glass window, it is only natural for the artist to place the thicker part at the bottom, as this is more aesthetically appealing and mechanically stable.

While the news of Zanotto's myth-busting result quickly spread across the world in popular science articles, one particularly astute reader (Gupta) noted that the extrapolation of Eq. (1) to room temperature provides only an upper limit to the actual room temperature viscosity since it does not account for the "isostructural" nature of glass below the transition temperature. In other words, Eq. (1) only provides an estimate for the equilibrium supercooled liquid viscosity, and the actual *nonequilibrium* viscosity of the glass can be much lower. Together, Zanotto and Gupta[5] published a revised estimate for the relaxation time of medieval stained glass at room temperature, this time on the order of 10^{23} years. While Zanotto's original conclusion that stained glass windows do not flow at room temperature still remains valid, the fact that the original estimate was a billion times too high points to the necessity of considering the nonequilibrium nature of dynamics below the glass transition.

It is thus apparent that an accurate description of the nonequilibrium viscosity of glass is essential for understanding low temperature relaxation.[6] Unfortunately, only a small number of such viscosity measurements have ever been performed since direct measurement of viscosity below the glass transition is often prohibitively time consuming[7–10] and expensive. Traditional atomistic modeling techniques such as molecular dynamics are even more restricted than experiment since they are generally limited by an integration time step on the order of 10^{-15} s,[11] which confines the total simulation time to $<10^{-6}$ s (at most).

Recently, we have developed a rigorous model for the glass transition range behavior of selenium, a simple elemental glass former.[12] Our model combines the enthalpy landscape approach[13–17] with nonequilibrium statistical mechanics techniques.[18–21] Our approach involves first mapping the continuous enthalpy landscape to a discrete set of inherent structures and transition points; this can be accomplished

using such techniques as eigenvector following[15,22] or activation relaxation.[23,24] A separate calculation is required to compute the inherent structure density of states.[25] Finally, the dynamics of the glass-forming system are computed using the master equation solver of Mauro *et al.*,[26] which employs a metabasin partitioning approach to access arbitrary time scales. Our model of selenium enables the accurate prediction of glass properties such as molar volume, heat capacity, shear viscosity, and fragility, without any empirical fitting parameters. The model itself has been validated against the experimental data of Varshneya and co-workers.[27,28]

In this paper, we apply the selenium landscape model to compute the nonequilibrium viscosity of glasses prepared over a wide range of cooling rates, 10^{-12}–10^{12} K/s. Nonequilibrium viscosity is lower for the faster cooling rates since the glass is trapped in a metabasin with more available transition paths, leading to a lower effective free energy barrier for structural transitions. Based on the landscape calculations for selenium, we propose a phenomenological model for nonequilibrium viscosity that provides accurate scaling over a wide range of temperatures and thermal histories. To validate the model we perform a series of measurements on Corning EAGLE XG™ glass over a range of temperatures and fictive temperatures. The measurements are performed using a specially designed beam-bending apparatus that enables accurate measurement of viscosity up to 10^{16} Pa s. The phenomenological model provides an accurate fit of nonequilibrium viscosity over the full range of temperatures and thermal histories. Finally, we investigate the impact of liquid fragility on glass viscosity, showing a direct connection between this equilibrium property and the parameters of the nonequilibrium viscosity model. In particular, we show that increased fragility leads to a sharper breakdown of ergodicity at the glass transition and a higher activation enthalpy for isostructural viscosity at low temperatures.

II. ENTHALPY LANDSCAPES AND THE GLASS TRANSITION

The study of glassy systems is made difficult by the three "*non*s:"

(1) Glass is *noncrystalline*, lacking the long-range atomic order found in most solid materials. Unlike crystalline materials, the structure of glass cannot be defined in terms of a simple unit cell that is repeated periodically in space.

(2) Glass is *nonequilibrium*; hence, the glassy state cannot be described using equilibrium thermodynamics or statistical mechanics. The macroscopic properties of a glass depend on both its composition and thermal history.

(3) Glass is *nonergodic* since we observe glass on a time scale that is much shorter than its structural relaxation time. As time elapses, ergodicity is gradually restored and the properties of a glass slowly approach their equilibrium values.[29–33]

At the heart of these issues lies the glass transition, i.e., the process by which an equilibrium ergodic liquid is gradually frozen into a nonequilibrium nonergodic glassy state. Modeling of the glass transition can be facilitated using the enthalpy landscape approach.[12–17] For an N-atom system, the enthalpy landscape is given by

$$H = U(\mathbf{r}_1, \mathbf{r}_2, \ldots, \mathbf{r}_N, L) + PL^3, \tag{2}$$

where the potential energy U is a function of the atomic position vectors $\mathbf{r}_1, \mathbf{r}_2, \ldots, \mathbf{r}_N$ and the length L is a function of the simulation cell. The pressure P of the system is constant and the simulation cell is assumed to be cubic. The H hypersurface is, in effect, a $(3N+1)$-dimensional landscape containing a multitude of local minima. Each of these minima corresponds to a mechanically stable configuration of atoms known as an "inherent structure."[34–39] The volume of configurational space that drains to a particular minimum via steepest descent is called a "basin;" there is one basin for every inherent structure.

The utility of the enthalpy landscape approach lies in the ability to separate the fast vibrations within a basin, i.e., the vibrations about a particular inherent structure configuration, from the slower interbasin transitions ("basin hopping"). While the landscape itself is independent of temperature, the way in which the system samples the landscape depends on its phonon energy and hence on the (phonon) temperature of the system. At high temperatures, the system can flow freely among basins, corresponding to the case of an ergodic equilibrium liquid. As the system is cooled, the interbasin transitions occur less frequently owing to the loss of thermal energy. Finally, the glassy state at low temperatures corresponds to a breakdown of ergodicity where the system becomes trapped in a subset of the overall phase space known as a "metabasin."[26,29]

In order to capture all memory effects in the glass, the full thermal history must be considered starting with the equilibrium liquid at a temperature well above the glass transition range (e.g., the melting temperature T_m). From equilibrium statistical mechanics, the initial probability of occupying any basin i is

$$p_i(0) = \frac{1}{Y(T_m)} g_i \exp\left(-\frac{H_i}{kT_m}\right), \tag{3}$$

where k is Boltzmann's constant, g_i is the degeneracy of basin i, H_i is its enthalpy, and Y is the isothermal-isobaric partition function,

$$Y(T_m) = \sum_{i=1}^{\Omega} g_i \exp\left(-\frac{H_i}{kT_m}\right). \tag{4}$$

The probabilities satisfy

$$\sum_{i=1}^{\Omega} p_i(t) = 1 \tag{5}$$

for all times t. The total number of nondegenerate basins is denoted Ω. For our model of selenium we employ the interatomic potentials of Mauro and Varshneya,[40] derived from quantum mechanics using Møller-Plesset perturbation theory[41] and the Dunning basis set.[42] Figure 1 shows the scaling of average enthalpy H_i and degeneracy g_i with the molar volume V_i of the inherent structures. Since we are interested only in the supercooled liquid and glassy states, crystalline inherent structures have been discarded. The enthalpy function $H(V)$ passes through a single minimum at

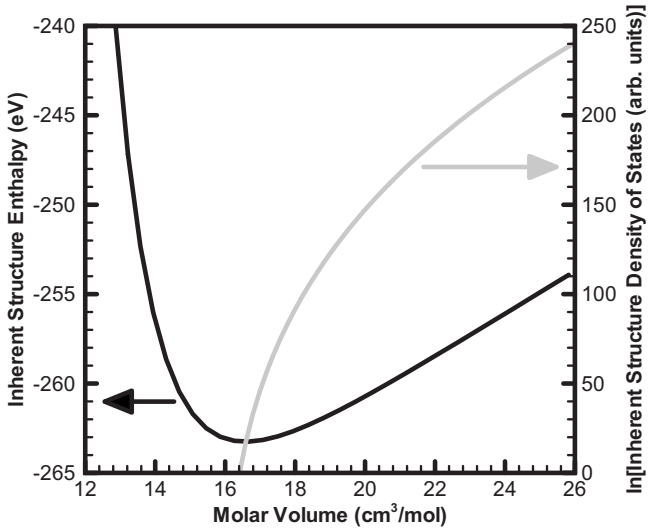

FIG. 1. Average inherent structure enthalpy and density of states as a function of molar volume. Only noncrystalline inherent structures are considered.

$V=V_{\min}$, which corresponds to the equilibrium volume of the supercooled liquid at absolute zero. Above $V_{\min}$, the degeneracy increases exponentially with enthalpy. The changes in molar volume exhibited by the liquid at different temperatures are the direct results of the competition between enthalpy effects, which drive the system toward $V_{\min}$, and degeneracy effects, which drive the system toward higher molar volumes. At high temperature, the degeneracy term dominates and we have a liquid with a high molar volume. As the temperature decreases the enthalpy term gradually becomes dominant, and the volume of the liquid contracts.

To model the dynamics of the system as it cools into the glass transition range, we construct a system of Ω coupled master equations,

$$\frac{dp_i(t)}{dt} = \sum_{j\neq i}^{\Omega} K_{ji}[T(t)]p_j(t) - \sum_{j\neq i}^{\Omega} K_{ij}[T(t)]p_i(t), \qquad (6)$$

where the rate parameters $K_{ij,ji}$ are defined parametrically in terms of an arbitrary cooling path, $T(t)$. Assuming transition state theory,

$$K_{ij}[T(t)] = \nu g_j \exp\left[-\frac{H_{ij}-H_i}{kT(t)}\right], \qquad (7)$$

where ν is the attempt frequency and H_{ij} is the transition point enthalpy.[26] For a sufficiently long isothermal hold, the solution of the master equation satisfies the detailed balance condition, and the system equilibrates giving a Boltzmann distribution of occupation probabilities. The transition points in selenium involve elementary bond angle and torsion angle transitions, which have a nearly constant enthalpy barrier of $\Delta H_{ij}=H_{ij}-H_i\approx 1$ eV (for $H_i>H_j$).[12,43] The molar volume of the glass can be computed at any time t with the phase space average,

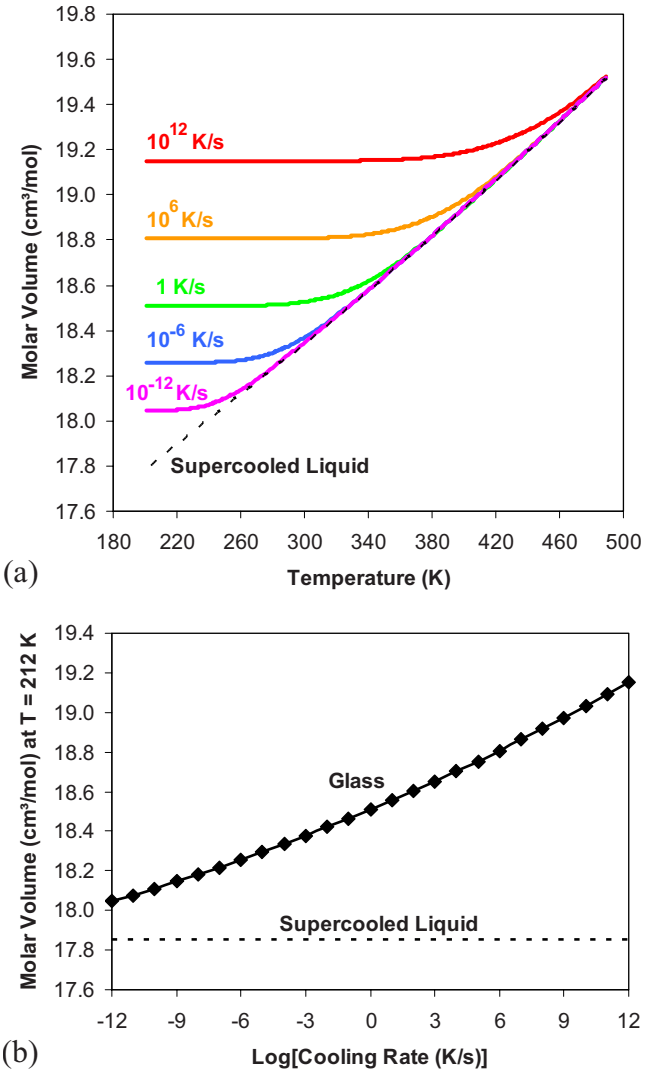

FIG. 2. (Color online) (a) Volume-temperature diagrams for five selenium glasses cooled from the melting temperature (T_m=490 K) to 200 K at rates of 10^{12}, 10^6, 1, 10^{-6}, and 10^{-12} K/s. The equilibrium supercooled liquid line is also shown. (b) Molar volume at T=212 K for cooling rates ranging from 10^{-12} to 10^{12} K/s. This temperature corresponds to T_g/T=1.5 for the 1 K/s cooled glass (which has T_g=318 K).

$$V(t) = \sum_{i=1}^{\Omega} V_i p_i(t). \qquad (8)$$

Figure 2(a) shows computed volume-temperature diagrams of selenium for linear cooling from the melting temperature (T_m=490 K) to 200 K. The cooling rate is varied from 10^{-12} to 10^{12} K/s. Faster cooling results in an earlier onset of the glass transition since the structure is given less time to equilibrate as the temperature is lowered. Figure 2(b) plots the glassy molar volumes at 212 K as a function of cooling rate. Full details of our enthalpy landscape model of selenium can be found in Ref. 12.

As derived previously,[12] the viscosity of a glass can be computed by

$$\eta(t_{obs}) = DNT\left[\sum_{i=1}^{\Omega} p_i \sum_{j\neq i}^{\Omega}\left(\sum_{k\neq j}^{\Omega} K_{kj} f_{ik}(t_{obs}) - \sum_{k\neq j}^{\Omega} K_{jk} f_{ij}(t_{obs})\right)\right]^{-1}, \quad (9)$$

where t_{obs} is the observation time (i.e., the measurement time), D is a constant related to the magnitude of the structural transitions, and $f_{ij}(t_{obs})$ is the conditional probability of occupying basin j after starting in basin i and evolving for exactly t_{obs}. The conditional probabilities account for basin hopping during the observation time window.[30] If we assume that the viscosity measurement is fast compared to the internal relaxation time scale of the glass, then the conditional probability f_{ij} reduces to a Kronecker delta function,

$$\lim_{t_{obs}\to 0} f_{ij}(t_{obs}) = \delta_{ij}, \quad (10)$$

and the viscosity expression becomes

$$\eta = DNT\left(\sum_{i=1}^{\Omega} p_i \sum_{j\neq i}^{\Omega} K_{ij}\right)^{-1}. \quad (11)$$

Substituting Eq. (7) into the above expression, we have

$$\eta[T(t)] = DNT\nu\left[\sum_{i=1}^{\Omega} p_i[T(t)] \sum_{j\neq i}^{\Omega} g_j \exp\left(-\frac{\Delta H_{ij}}{kT(t)}\right)\right]^{-1}. \quad (12)$$

Equation (12) is valid in the "landscape-dominated" regime below the critical temperature T_c predicted by mode-coupling theory.[38,44,45] In this temperature regime, which starts in the supercooled liquid state above the glass transition, the dynamics are characterized by multiple vibrations inside a basin with less frequent interbasin transitions. In this manner, the system loses memory between successive basin hoppings, and the system follows Markov chain dynamics among the network of basins.

Figure 3(a) plots the viscosity of selenium glass cooled at different rates. The constant D is chosen such that $\eta = 10^{12}$ Pa s at the computed glass transition temperature of the 1 K/s cooled glass ($T_g = 318$ K).[12,46] As expected, a faster cooling results in an earlier glass transition and a glass with higher molar volume. As shown in Fig. 1, the inherent structures with higher molar volume also have higher degeneracy factors and hence a greater number of available transitions. This corresponds to a lower effective free energy barrier for structural relaxation, and hence a faster cooled glass will generally exhibit a lower viscosity compared to a more slowly cooled glass. This scaling of nonequilibrium viscosity with cooling rate is shown clearly in Fig. 3(b).

Figure 4 plots the relaxation of glass viscosity toward its equilibrium supercooled liquid value. The relaxation is shown for the 1 K/s cooled glass under an isothermal hold at $T_g/T = 1.5$ ($T = 212$ K). The viscosity relaxes from $10^{27.05}$ to $10^{27.26}$ Pa s on a time scale of minutes. On a time scale of years, the viscosity relaxes to $10^{29.0}$ Pa s. We note that the glass *appears* to equilibrate on both of the time scales in parts (a) and (b) in Fig. 4. However, full equilibration of the system to the supercooled liquid viscosity of $10^{32.2}$ Pa s occurs on the time scale of billions of years.

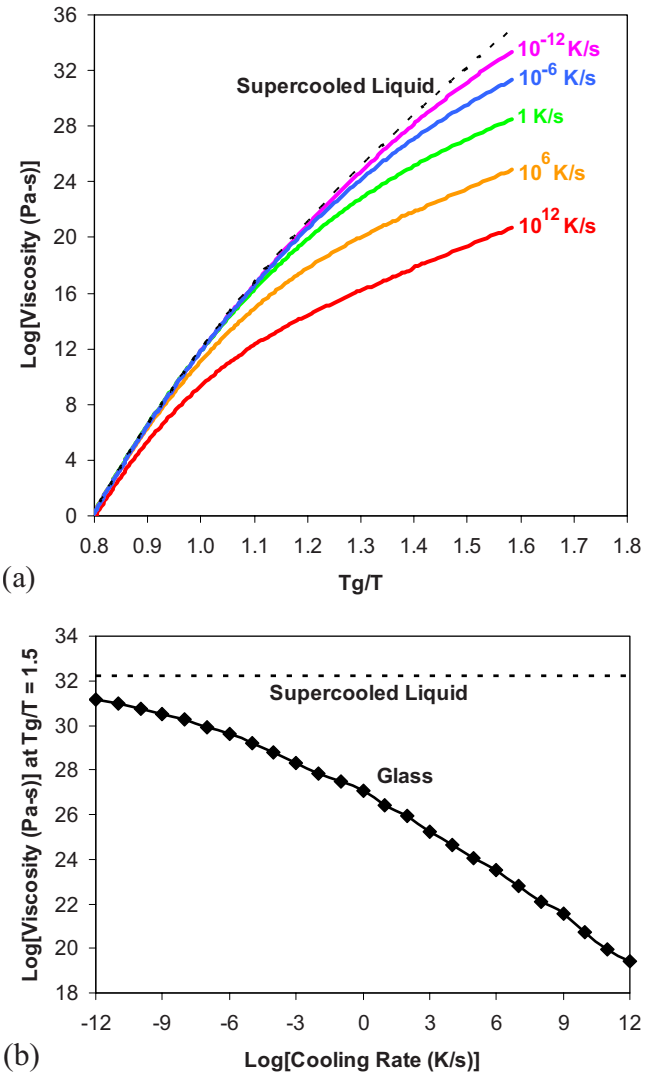

FIG. 3. (Color online) (a) Plot of $\log_{10}\eta$ as a function of T_g/T for selenium glass prepared using cooling rates of 10^{-12}, 10^{-6}, 1, 10^{6}, and 10^{12} K/s. For plotting purposes we consider a reference glass transition temperature of $T_g = 318$ K, which corresponds to the 1 K/s cooled glass. The equilibrium supercooled liquid line is also shown. (b) Plot of $\log_{10}\eta$ at $T_g/T = 1.5$ ($T = 212$ K) for selenium with linear cooling rates ranging from 10^{-12} to 10^{12} K/s.

III. PHENOMENOLOGICAL MODELS OF NONEQUILIBRIUM VISCOSITY

While the enthalpy landscape approach enables calculation of nonequilibrium viscosity from first-principles physics, it is impractical to compute the full enthalpy landscape of every new glass-forming composition. In addition, the lack of accurate interatomic potentials poses a severe limitation for most inorganic glasses.[11] It is therefore desirable to have an accurate phenomenological model of glass viscosity that captures the essential physics with some small number of empirical fitting parameters.

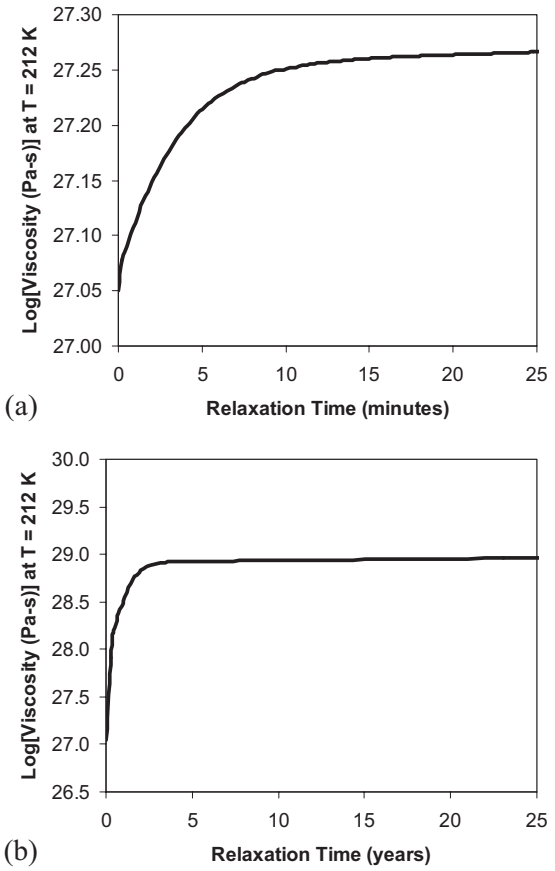

FIG. 4. Relaxation of $\log_{10}\eta$ of selenium glass toward the equilibrium supercooled liquid value at $T=212$ K ($T_g/T=1.5$). The selenium glass was prepared using a cooling rate of 1 K/s and relaxation is shown on the time scale of (a) minutes and (b) years. Full equilibration occurs on a time scale of billions of years.

Phenomenological models generally consider nonequilibrium viscosity to be a function of both the physical (phonon) temperature T and the fictive temperature T_f,

$$\eta = \eta(T, T_f). \tag{13}$$

While the definition of fictive temperature varies from author to author,[47,48] when studying volume relaxation behavior it is convenient to define T_f as the temperature of the supercooled liquid where the molar volume is the same as that of the glass.[47] Written in terms of the enthalpy landscape approach, fictive temperature can be defined by

$$\sum_{i=1}^{\Omega} V_i p_i[T(t)] = \frac{1}{Y(T_f)} \sum_{i=1}^{\Omega} V_i g_i \exp\left(-\frac{H_i}{kT_f}\right), \tag{14}$$

where the left-hand side of the equation gives the molar volume of the glass accounting for the full thermal history and the right-hand side is the equilibrium molar volume at T_f. Note that this equation is for the configurational molar volume only; the vibrational contribution has been factored out. In practice, we fit the right-hand side of the equation to a second-order polynomial in T_f and then use the quadratic formula to solve for T_f as a function of the cooling path $T(t)$. Figure 5(a) shows the computed fictive temperature of the glass at $T=212$ K as a function of cooling rate. Figure 5(b) plots molar volume as a function of fictive temperature

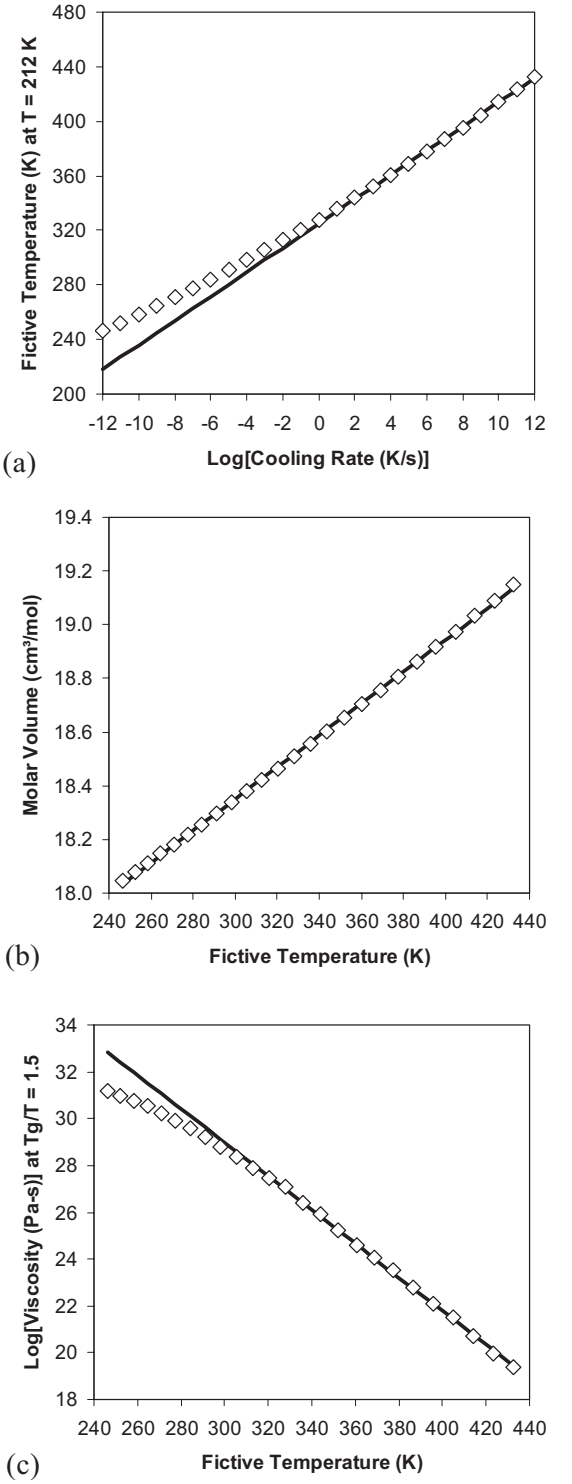

FIG. 5. (a) Fictive temperature, T_f, for selenium after cooling from the melting temperature (490 K) to 200 K with linear cooling rates ranging from 10^{-12} to 10^{12} K/s. (b) Molar volume as a function of fictive temperature (equals supercooled liquid volume as a function of temperature). (c) $\log_{10}\eta$ at $T_g/T=1.5$ ($T=212$ K) as a function of fictive temperature of the glass. In all plots, the solid line shows a linear fit in the high fictive temperature regime.

(equivalent to plotting supercooled liquid volume as a function of physical temperature). Finally, Fig. 5(c) plots the nonequilibrium viscosity at $T=212$ K as a function of fictive temperature. The logarithm of viscosity scales linearly with fictive temperature except at very low values of fictive temperature (corresponding to very slow cooling rates).

One popular expression for glass viscosity is that of Narayanaswamy,[49]

$$\eta_N = \eta_\infty \exp\left[f\frac{\Delta H_N}{kT} + (1-f)\frac{\Delta H_N}{kT_f}\right], \quad (15)$$

where ΔH_N is a constant activation barrier and f is a constant satisfying $0 \leq f \leq 1$. At equilibrium the fictive temperature is equal to the physical temperature ($T_f=T$) and the Narayanaswamy equation reduces to an Arrhenius form. Hence, this model is not capable of accounting for the non-Arrhenius scaling of viscosity exhibited by fragile systems at equilibrium.[46]

A second phenomenological expression for glass viscosity can be derived from the Adam-Gibbs equation,[50] which relates the viscosity to the configurational entropy S_c of the system,

$$\eta_{AG} = \eta_\infty \exp\left(\frac{A}{TS_c(T,T_f)}\right). \quad (16)$$

Here, A is a constant and the configurational entropy S_c is a function of both the physical temperature T and fictive temperature T_f. This expression can be simplified[6] by assuming

$$S_c = \int_{T_K}^{T_f} \frac{\Delta C_p}{T} dT, \quad (17)$$

where T_K is the hypothetical Kauzmann temperature at which the configurational entropy is zero.[51] The quantity $\Delta C_p = C_{pl} - C_{pg}$ is the difference between the isobaric heat capacities of the liquid and glassy states. Near the glass transition range, ΔC_p is found experimentally to scale about linearly with temperature,

$$\Delta C_p = C_0 + C_1 T. \quad (18)$$

Defining $Q = Ak/C_0$ and $C = C_1/C_0$, we have the following expression for glassy viscosity in the Adam-Gibbs framework:[6]

$$\eta_{AG} = \eta_\infty \exp\left[\frac{Q/kT}{\ln(T_f/T_K) + C(T_f - T)}\right]. \quad (19)$$

Please note that the validity of Eq. (17) has recently been challenged at several levels.[30,47,52–55]

A third popular expression for nonequilibrium viscosity is the Mazurin equation,[56–58]

$$\log_{10}\ \eta_M = \left(\frac{T_f}{T}\right)\log_{10}\ \eta_{eq}(T_f) + \left(1 - \frac{T_f}{T}\right)\log_{10}\ \eta_0, \quad (20)$$

where η_0 is a constant and η_{eq} is the equilibrium viscosity function, commonly expressed in terms of the VFT form of Eq. (1). Note that η_{eq} is evaluated at the fictive temperature T_f where the glass structure is considered to be "frozen;" this serves as the base point from which the isostructural viscosity is extrapolated. In this way Eq. (20) avoids the singularity of the VFT equation in Eq. (1) since for all practical systems the fictive temperature T_f freezes in at some value well above T_0. (At equilibrium, $T_f=T$.) A key advantage of the Mazurin expression is that it divides the glass viscosity equation into separate equilibrium and nonequilibrium terms, where the equilibrium piece can adopt any desired form; it is not necessary to use VFT. Hence, the Mazurin equation offers the flexibility to choose the most appropriate form of η_{eq} for the system under study, and the parameters for η_{eq} can be fitted separately from the nonequilibrium η_0 parameter.

Finally, a fourth expression for nonequilibrium viscosity is due to Avramov,[59]

$$\eta_A = \eta_\infty \exp\left[\left(\frac{\theta}{T_f}\right)^a \left(\frac{T_f}{T}\right)^g\right], \quad (21)$$

where θ, a, and g are fitting parameters. In the limit of $T=T_f$, Eq. (21) reduces to the Avramov-Milchev (AM) equation[60] for equilibrium viscosity. Recent studies have shown that the AM equation provides a poor description of high temperature viscosity due to a divergence of configurational entropy.[55,61]

Figure 6 shows best fits of the above Narayanaswamy, Adam-Gibbs, Avramov, and Mazurin expressions to the computed viscosity of selenium glass from Sec. II. The viscosities shown in Fig. 6(a) are for the 1 K/s cooled glass as a function of T_g/T, where $T_g=318$ K. Here we have applied a correction to the equilibrium viscosity calculation above the mode-coupling temperature (i.e., at temperatures above the landscape-dominated regime), leading to the "s-shaped" viscosity curve as described in Ref. 12. The fictive temperature T_f varies with physical temperature according to Eq. (14). Of the four models, only the Mazurin expression of Eq. (20) can provide an accurate fit of equilibrium viscosity at temperatures above T_g since it allows for independent control of the equilibrium and nonequilibrium terms. Below T_g, all three models yield approximately Arrhenius scaling of viscosity with temperature, such as computed in the isostructural regime at very low temperatures. However, none captures the shape of the viscosity curve during the glass transition itself. Figure 6(b) shows the model fits as a function of fictive temperature given a constant physical temperature of $T_g/T=1.5$ ($T=212$ K). The Mazurin expression provides an accurate fit over a narrow range of T_f values; however, it significantly overestimates viscosity at both higher and lower values of fictive temperatures. The Narayanaswamy, Adam-Gibbs, and Avramov expressions exhibit a more accurate scaling of viscosity over a wider range of fictive temperatures.

We have found that the Mazurin expression of Eq. (20) can be improved with a simple modification as below,

$$\log_{10}\ \eta_{MM} = \left(\frac{T}{T_f}\right)\log_{10}\ \eta_{eq} + \left(1 - \frac{T}{T_f}\right)\log_{10}\ \eta_0. \quad (22)$$

In this modified Mazurin equation, we have simply inverted the T_f/T factors in the original Mazurin expression of Eq. (20). The rationale for this inversion is that the fictive temperature T_f is greater than the physical temperature T for any

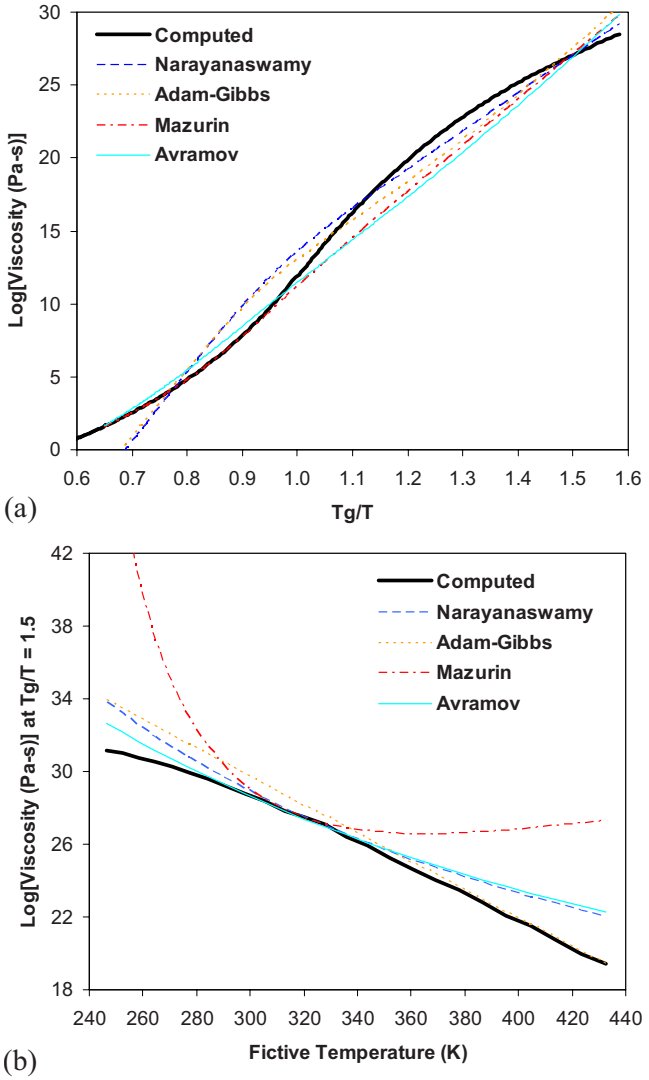

FIG. 6. (Color online) Computed $\log_{10}\eta$ of selenium using the enthalpy landscape approach and fit with the Narayanaswamy, Adam-Gibbs, Mazurin, and Avramov expressions of Eqs. (15) and (19)–(21), respectively. (a) Viscosity as a function of normalized inverse temperature for selenium glass cooled at a rate of 1 K/s. (b) Viscosity as a function of fictive temperature for selenium glass at $T_g/T=1.5$ ($T=212$ K). Fictive temperature is computed using Eq. (14).

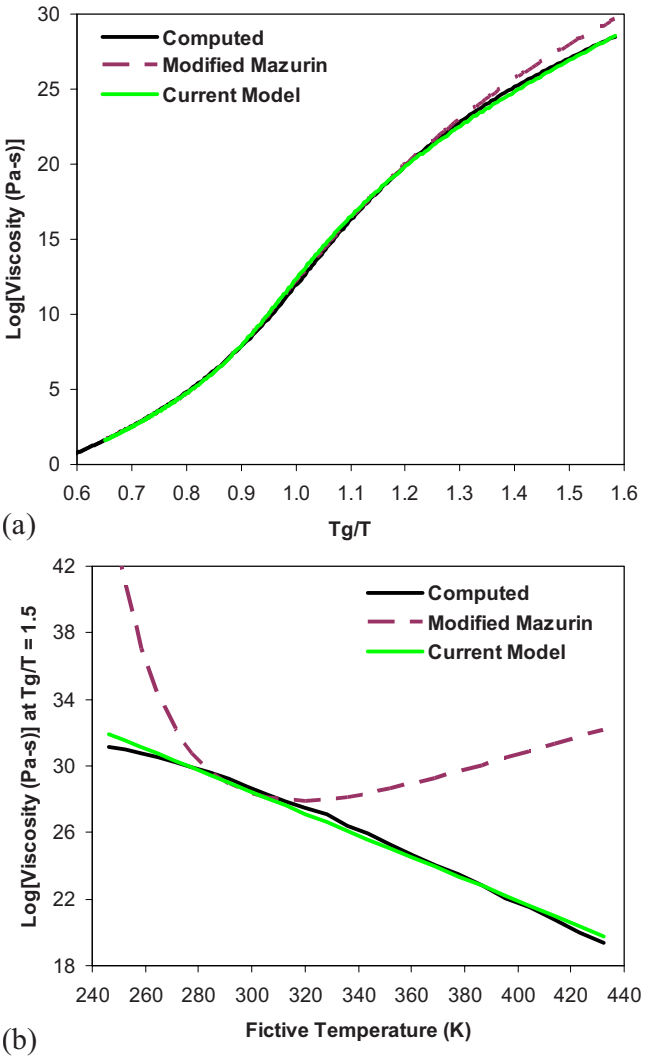

FIG. 7. (Color online) Computed $\log_{10}\eta$ of selenium using the enthalpy landscape approach and fit with the modified Mazurin expression of Eq. (22) and our current nonequilibrium viscosity model of Eq. (23). (a) Viscosity as a function of normalized inverse temperature for selenium glass cooled at a rate of 1 K/s. (b) Viscosity as a function of fictive temperature for selenium glass at $T_g/T=1.5$ ($T=212$ K). Fictive temperature is computed using Eq. (14).

normally cooled glass. Hence, the ratio T/T_f satisfies $0\leq T/T_f\leq 1$. At equilibrium $T=T_f$, so the ratio is unity; in the glassy state $T_f>T$ (typically), so the ratio is less than unity and decreases with decreasing T. Hence, the ratio T/T_f is a measure of how close the system is to equilibrium. Likewise, the $1-T/T_f$ factor in the second term of Eq. (22) gives the degree of departure from equilibrium. Under special circumstances such as a long isothermal hold followed by a fast upquench, the fictive temperature can actually be lower than the physical temperature ($T_f<T$). Hence, in the generalized case one should replace T/T_f with $\min(T,T_f)/\max(T,T_f)$ such that the ratio is always less than unity and a reflection of the system's closeness to equilibrium. As shown in Fig. 7(a), this simple modification to the Mazurin expression enables a much closer fit to the computed viscosity-temperature data, as compared to the original Mazurin expression in Fig. 6(a). However, Fig. 7(b) shows that the modified Mazurin expression does not provide any advantage when considering the scaling of viscosity with T_f at fixed T.

IV. IMPROVED PHENOMENOLOGICAL MODEL OF GLASS VISCOSITY

Figure 6 shows that none of the phenomenological models from Sec. IV provides an accurate description of nonequilibrium viscosity. It is therefore desirable to introduce a model satisfying the following criteria:

(1) A single expression should be used to describe the equilibrium and nonequilibrium regimes. In other words, the nonequilibrium viscosity model should reduce to an established equilibrium form for $T=T_f$.

(2) The model should provide an accurate scaling of viscosity through the glass transition range, accounting for the continuous nature of the glass transition.

(3) In the low temperature (i.e., fully nonergodic) limit the model should reduce to an Arrhenius form reflecting the isostructural viscosity.

(4) The model should be applicable over a wide range of fictive temperatures (i.e., thermal histories).

To this end, we introduce the following phenomenological model of viscosity:

$$\log_{10}\ \eta(T,T_f) = x\ \log_{10}\ \eta_{eq}(T_f) + (1-x)\log_{10}\ \eta_{ne}(T,T_f), \tag{23}$$

where x is an ergodicity parameter defined by

$$x = \left(\frac{\min(T,T_f)}{\max(T,T_f)}\right)^p. \tag{24}$$

For a typical system where $T_f \geq T$, Eq. (24) simplifies to

$$x = \left(\frac{T}{T_f}\right)^p. \tag{25}$$

The form of the viscosity expression above mirrors that of the modified Mazurin expression in Eq. (22). However, we introduce a new p parameter governing the sharpness of ergodic breakdown as the system is cooled through the glass transition range. In Sec. VII we will show that p scales linearly with the supercooled liquid fragility m. As with the Mazurin approach, η_{eq} can be given by the VFT expression or another form more suitable to the particular system under study. We generally employ the Mauro-Yue-Ellison-Gupta-Allan (MYEGA) equation for equilibrium viscosity,

$$\log_{10}\ \eta_{eq}(T_f) = \log_{10}\ \eta_\infty + \frac{C}{T_f}\exp\left(\frac{K}{T_f}\right), \tag{26}$$

where C and K are constants for a given composition. Previously we have shown that Eq. (26) provides an improved description of equilibrium viscosity compared to both VFT and AM.[55]

For the nonequilibrium viscosity $\eta_{ne}(T,T_f)$ in Eq. (23), we adopt the form

$$\log_{10}\ \eta_{ne} = \frac{\Delta H}{kT\ \ln\ 10} + A - BT_f, \tag{27}$$

where ΔH, A, and B are constants for a given glass composition. The first term of Eq. (27) provides Arrhenius scaling of glass viscosity in the isostructural regime (where T_f becomes frozen at some constant value). Here, ΔH is the activation enthalpy for isostructural flow. The next two terms, $A-BT_f$, account for the linear scaling of $\log_{10}\ \eta(T,T_f)$ with T_f for a fixed T.

As shown in Fig. 7, our current phenomenological model of glass viscosity provides an excellent fit to the computed viscosity data over the full ranges of T and T_f. Next we will show validation of the model against measured nonequilibrium viscosity data for Corning EAGLE XG™ glass.

V. EXPERIMENTAL PROCEDURE

A modified beam-bending apparatus together with an in-house developed data acquisition system was used to measure viscosity. Using deflection measurements of a simply supported beam, the method is suitable for determining viscosity in the approximate range of 10^8–10^{16} Pa s. Deflection $y(t)$ and viscosity $\eta(t)$ are related by[7,62]

$$y(t) = C\int_0^t \frac{dt'}{\eta[T,T_f(t')]}. \tag{28}$$

In this expression $y(t)$ is the deflection of the midpoint of the beam at time t, η is the viscosity, and the constant C incorporates the load hanging on the beam and its geometry with the expression

$$C = \frac{gL^3}{120wh^3}\left[M_{load} + \frac{\rho whL}{1.6}\right]. \tag{29}$$

The above expression is used in standard beam-bending viscometry.[62] It may be derived by superposing the elementary textbook solutions[63] for the deflection of a simply supported beam loaded at the center and a simply supported beam uniformly loaded and using the "viscoelastic analogy" (see Ref. 7, pp. 213 and 214) to replace shear strain by shear strain rate and to replace shear modulus by shear viscosity and treat the viscous flow as incompressible. Here, g is the acceleration of gravity in $\mathrm{cm/s^2}$, ρ is the density of the glass bar in $\mathrm{g/cm^3}$, M_{load} is the total load mass in grams, L is the span or distance between supports, w is the width, and h is the (vertical) thickness of the beam. All of the lengths are measured in cm such that the resulting C is in units of Pa cm. The thermocouple was housed in a double-bore alumina tube with its junction placed within 1.0 cm of the specimen near the axis of the furnace. The emf was measured with the Watlow F4 electronic thermometer. The Watlow calibration was verified using a Micromite II calibrator with NIST traceable certificate. Both devices had a sensitivity of 0.1 °C and an accuracy of 0.5 °C.

The experiments started by placing the double polished flat beam specimen onto a ceramic support stand in the "hot zone" of the furnace at room temperature. Sample geometry for all work was $h=0.07$ cm thick, $w=0.3$ cm wide, and 10 cm long. A fused silica rod flame bent at one end in the form of a shepherd's crook was used to place a load on the specimen. It was placed in the middle of the furnace and attached to the rig by hold-release mechanism underneath the furnace. This hold-release setup prevented loading of the sample and associated deflection due to weight of the fused silica rod during the initial heating state of the experiment. The total load consisted of the combined weight of the fused silica rod, the small fixtures, and the core of the linear variable differential transformer (LVDT). The ceramic support stand was of rectangular shape and made from an alumina muffle with two notches. The inside edges of these notches define the support span for the specimen. The span of these edges was $L=5.2$ cm. Both notches have flat supporting surfaces covered by Pt foil to prevent sticking of the glass to the alumina muffle as the temperature rises. The furnace was programmed to achieve the time-temperature function of inter-

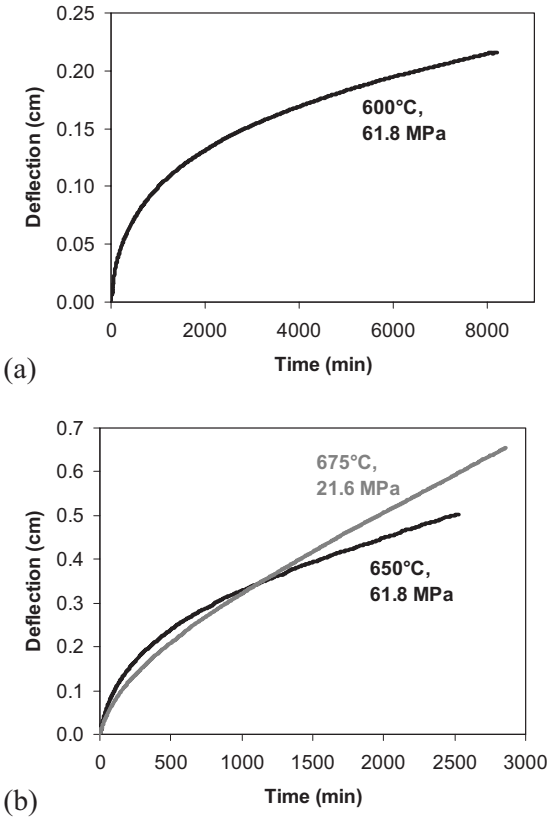

FIG. 8. Experimental results of deflection at the center of the EAGLE XG™ flat beam as a function of time. Experiments were conducted isothermally at (a) 600 °C using an applied uniaxial stress of 61.8 MPa, (b) 650 °C using a stress of 61.8 MPa, and 675 °C using a stress of 21.6 MPa.

est. The initial heating rate was 10 K/min up to a temperature approximately 10 °C below the final temperature, at which time the hold-release mechanism was activated so that the total load was applied at the center of the beam. The experiment continued by slowing down the heating rate to 3 K/min to reach the final temperature T_{final}, followed by an isothermal segment where the deflection measurement was conducted. Measurements were carried out over extended periods of time at predetermined final temperatures (viz., 600, 650, and 675 °C). Since the hook was attached to the core of the LVDT by small fixtures, we can observe this deformation and record it using the data acquisition system.

Figure 8 shows examples of such recorded experiments on EAGLE XG™ glass. In each case the uniaxial stress was applied in the center of the flat beam. Figure 8(a) shows results for the 600 °C measurement, where the applied stress was equal to 61.8 MPa. Based on recorded deflection data, we can see that the viscosity does not represent conditions of equilibrium at the beginning of the measurement where the deflection curve is clearly nonlinear. [Equation (28) shows that the slope of the deflection curve is proportional to the reciprocal of nonequilibrium viscosity.] The nonlinearity is presumed to be due to glass relaxation that proceeds during the measurement. The slope of deformation vs time of the loaded sample begins to approach more closely a constant value near the end of the experiment, i.e., 136 h, but we will show in Sec. VI that the viscosity is still evolving even after 136 h at 600 °C. Two other temperature values, 650 and 675 °C, were chosen in order to measure deformation of the dimensionally identical but separate beams at higher temperatures. The uniaxial stress applied in the center of the flat beam at the lower temperatures was equal to 61.8 MPa whereas at the temperature of 675 °C the stress was 21.6 MPa in order to achieve longer observation time due to low viscosity-high deformation rate conditions at this temperature. Deflection curves for the 650 and 675 °C experiments are shown in Fig. 8(b). Note that in every deflection vs time curve, the curvature is concave downward. This may at first seem surprising but it is a simple consequence of isothermal glass relaxation. While being held at a fixed temperature, the glass undergoes relaxation from a condition far from equilibrium (with its lower viscosity) to a condition closer to equilibrium (with its higher viscosity). As Eq. (28) makes clear, the slope of the isothermal deflection curve has to diminish as the viscosity increases as equilibrium is approached.

Note that all experiments provide sufficient amount of data for statistically relevant analyses at all viscosity data ranges, i.e., between $10^{13.5}$ and $10^{15.9}$ Pa s attainable by using this isothermal beam-bending method. At the highest measured temperature of 675 °C, the slope of the deflection curve [Fig. 8(b)] is the most constant, representing the closest approach to equilibrium viscosity. This is to be expected since the rate of equilibration is approximately set by the reciprocal of viscosity, which itself is strongly temperature dependent.

VI. MODEL VALIDATION

Fitting the various phenomenological models to the experimentally measured beam deflection data of EAGLE XG™ glass involves a number of steps:

(1) Estimate the time-dependent fictive temperature $T_f(t)$ based on the sample thermal history and measured glass strains.

(2) Given a trial set of model parameters, calculate the time-varying nonequilibrium viscosity and use it to predict deflection of the beam for all three temperatures that were measured.

(3) Vary the parameters of each model until the agreement between predicted and measured beam deflection is optimized. Note that we use a single set of viscosity parameters to match beam deflection data simultaneously at all three temperatures.

The models described in Secs. III and IV are formulated as functions of temperature T and fictive temperature T_f. While each experiment is conducted isothermally, the fictive temperature T_f will evolve toward the furnace temperature with time and the relaxation of T_f will be different at each temperature (e.g., faster relaxation at higher temperature). The initial value of fictive temperature (prior to starting the beam deflection measurement) is set by the thermal history of the glass manufacture and is the same for all samples. This initial fictive temperature is determined by calorimetry measurements using the area matching method of Yue *et al.*[64] The subsequent evolution of fictive temperature is estimated

from the known thermal history of the beam sample (its temperature curve from room temperature to the temperature of the experiment) and its constant temperature during the measurement. That estimate is based on measurements of glass strain $\Delta L/L$ or compaction for thermal cycles that are close in temperature to the beam deflection measurement temperatures (600, 650, and 675 °C) and use of a phenomenological compaction model to interpolate times and temperatures. This estimate assumes a linear relation between change in fictive temperature and glass strain observed at room temperature, i.e.,

$$\frac{\Delta L}{L} = \alpha_f \Delta T_f, \tag{30}$$

where $\Delta L/L$ is a change in length divided by initial length (strain), α_f is a fictive thermal expansion coefficient, and ΔT_f is a change in fictive temperature. This relation is equivalent to a linearized version of the fictive temperature definition in Eq. (14). We interpolate model values of $T_f(t)$ onto the set of times at which beam deflections were measured (every 1 or 2 min); these values of $T_f(t)$ are used in nonequilibrium viscosity calculations.

The time-varying nonequilibrium viscosity is calculated using each of the phenomenological models, together with the constant T of the experiment and the $T_f(t)$ curves described above. While it would be convenient to compare and fit model viscosities with viscosities extracted directly from the beam deflection equation [using Eq. (28)], the derivative of deflection vs time calculated by numerical differences is noisy. The deflection curves themselves, viewed over the full time history, look very smooth, but the individual measurements every 1–2 min contain small measurement noise. To avoid amplifying noise when fitting a model to measured data, it is standard procedure to avoid taking numerical differences and work instead with integral forms of the model and data. Thus we perform model fits based on measured *deflections* instead of viscosities. However, we can also extract an approximate time-varying viscosity directly from deflection data by fitting a smooth empirical time-dependent viscosity function of the simple form

$$\eta(t) = \eta_{eq} + (\eta_0 - \eta_{eq})e^{-t/\tau}. \tag{31}$$

This is the simplest empirical expression that contains enough flexibility to represent an initial value of viscosity given by η_0, a final equilibrium value being approached at infinite time given by η_{eq}, and a time scale for the relaxation of viscosity given by τ. This expression has the fortunate property that $1/\eta(t)$ can be integrated exactly as in Eq. (28) to give the deflection in the form

$$y(t) = \frac{C}{\eta_{eq}}\left[t + \tau \ln\left(\frac{1 + (\eta_0/\eta_{eq} - 1)\exp(-t/\tau)}{\eta_0/\eta_{eq}}\right)\right]. \tag{32}$$

This equation has been shown in a previous publication[65] to give an excellent fit to beam deflection data for two different glasses and several temperatures. One might have expected a stretched exponential behavior for the time relaxation of viscosity but the above expression matches the measured data so well that we did not pursue using a stretched exponential. Note that this is not really a viscosity *model* but only a convenient approximate representation of time-varying viscosity at a single temperature. The three constants of this expression are fit separately at every temperature of interest.

We fit deflection curves starting at 20 min after the beam reaches its target temperature to ensure that the sample has reached a stable temperature and that any initial transient is small enough to ignore. The 20 min is included in the thermal history used to calculate $T_f(t)$ but is ignored when comparing deflection curves. This small 20 min time interval is much shorter than the measurement times of 2530–8200 min. Deflection is calculated from nonequilibrium viscosity using Eq. (28). For the various viscosity models, the integral in Eq. (28) is performed numerically using time steps equal to the measurement time intervals of 1 or 2 min.

Model parameters are optimized against measured deflection data using a Levenburg-Marquardt optimization algorithm.[66] We use a penalty function defined as the sum of squares of differences between calculated and measured deflections. In order to interpret the square root of the overall penalty function as a root-mean-square error, we combine the sum of squares in a weighted sum over the three temperatures with weights that add to unity but rescale the penalties at each temperature by the maximum deflection. The equation for the optimization penalty is

$$P^2 \equiv \left(\frac{1}{y_{600}^2}\frac{\chi_{600}^2}{N_{600}} + \frac{1}{y_{650}^2}\frac{\chi_{650}^2}{N_{650}} + \frac{1}{y_{675}^2}\frac{\chi_{675}^2}{N_{675}}\right) \Bigg/ \left(\frac{1}{y_{600}^2} + \frac{1}{y_{650}^2} + \frac{1}{y_{675}^2}\right), \tag{33}$$

where each y_T represents the maximum deflection at temperature T, N_T is the number of data points at temperature T, and each χ_T^2 is defined by

$$\chi_T^2 \equiv \sum_{i=1}^{N_T} [y_i - y_{\text{model}}(t_i)]^2. \tag{34}$$

In this expression y_i are the measured deflections and $y_{\text{model}}(t_i)$ are the corresponding model deflections. With this definition P can be interpreted as an overall rms error in the fit for all three temperatures. Please note that the Levenburg-Marquardt algorithm gives only a local minimum in the penalty function; in order to assess the robustness of the fit and seek a global optimum for each model, we restarted the optimizations about 10^4 times each using a random number generator to choose initial starting values. The final fits we report are reliable global minima.

In order to facilitate comparison among models, we rewrote each viscosity expression in terms of a common set of parameters: $\log_{10}\eta_\infty$, fragility m, and glass transition temperature T_g. (Fragility and glass transition temperature are defined formally at the beginning of Sec. VII.) For example, the Avramov viscosity of Eq. (21) can be rewritten as

TABLE I. Summary of fitting parameter values and values of best-fit rms error for various nonequilibrium viscosity models and optimal parameter sets. Details and symbols are described in the text. Experimental values for three parameters are given on the last row. All viscosities are in units of Pa s. The rms error is described in the text and is given in cm.

Viscosity model	$\log_{10}(\eta_\infty)$	Fragility m	T_g (°C)	$\log_{10}(\eta_0)$	g	p	A	$\Delta H/(k \ln 10)$	B	f	rms error
Narayanaswamy		24.9	772.9							0.666	0.135
Mazurin with VFT	−3	23.3	774.3	−4.397							0.133
Mazurin with MYEGA	−3	23.8	773.3	−4.511							0.132
Mod. Mazurin with MYEGA	−3	28.6	760.6	34.71							0.138
Avramov	−3	24.3	772.9		1.093						0.130
Current with VFT	−3	32.1	735.5			6.91	50.0	7653	0.0390		0.00468
Current with MYEGA	−3	32.5	735.7			6.32	52.7	6853	0.0404		0.00467
Experimental data		36.2	741.1								

$$\log_{10}\eta_A(T,T_f) = \log_{10}\eta_\infty + (12-\log_{10}\eta_\infty)\left(\frac{T_g}{T_f}\right)^{m/(12-\log_{10}\eta_\infty)} \times\left(\frac{T_f}{T}\right)^g. \quad (35)$$

All models share these common parameters except the Narayanaswamy model, which has only two of the three,

$$\log_{10}\eta_N(T,T_f) = (12-m) + \frac{mT_g f}{T} + \frac{mT_g(1-f)}{T_f}. \quad (36)$$

The Mazurin, modified Mazurin, and current model all have an independent equilibrium viscosity term (see Secs. III and IV), which we formulate in terms of either the VFT equation,

$$\log_{10}\eta_{eq,\mathrm{VFT}}(T_f) = \log_{10}\eta_\infty + \frac{(12-\log_{10}\eta_\infty)^2}{m(T_f/T_g-1)+(12-\log_{10}\eta_\infty)}, \quad (37)$$

or the MYEGA equation,

$$\log_{10}\eta_{eq,M}(T_f) = \log_{10}\eta_\infty + (12-\log_{10}\eta_\infty)\frac{T_g}{T_f} \times\exp\left[\left(\frac{m}{12-\log_{10}\eta_\infty}-1\right)\left(\frac{T_g}{T_f}-1\right)\right]. \quad (38)$$

The results of these parameter fitting optimization exercises are summarized in Table I. The rms error quoted in Table I is the value P defined in Eq. (33) above. As expected, the VFT and MYEGA versions give similar results in terms of the three parameters given above. For every case the $\log_{10}\eta_\infty$ parameter was fixed at the indicated value in Table I while all other parameters were adjusted to their optimal value. (Since we do not include high temperature viscosity data in the penalty function, the fit qualities are insensitive to the particular value of $\log_{10}\eta_\infty$.)

All models except the current model obtain a fragility parameter m that is much too low (about 24) compared with direct experimental measurement (36), while the current model gets about 32. All the models except the current model obtain a glass transition temperature T_g that is too large compared with the experimental value (obtained by fitting measured equilibrium viscosity data). Of course, the most glaring result of Table I is that the current model has a substantially smaller value of the penalty function compared with the other models. This is seen dramatically in Figs. 9–11, where we compare the models to the measured deflection curves and viscosities.

The best fit deflection curves are shown in Fig. 9 for the three temperatures. In each plot [(a)–(c)] there is a black curve that shows the measured deflection data. This is somewhat covered by the empirical fit [Eq. (32)] and by the current nonequilibrium viscosity model, both of which give excellent fits to the deflection data at all three temperatures. All the other models under consideration fail to agree with the deflection curves, especially at the lower temperatures. We infer that none of these models adequately represents the fictive temperature dependence of nonequilibrium viscosity, and the failure becomes aggravated further from equilibrium at the lowest temperature studied. It is interesting that all of these models fail in approximately the same way, probably from their inability to account for a realistic continuous glass transition.

Another view comparing model and measured results is given in Fig. 10, where the model viscosity is compared with the empirical viscosity inferred from Eq. (31), plotted against the fictive temperature. Again the current model has the higher slope vs T_f that is also seen in the empirical fit, while all the other models have too low slope, especially at 600 °C. Once again all the other models share the same behavior that misses the measured trend, and the discrepancy is worst at the lowest temperature. Please note that at low fictive temperatures the $\log_{10}\eta(T_f)$ becomes slightly curved, especially for the 675 °C experiment. This is consistent with our result for selenium in Fig. 5(c) and indicates that the system is still within the glass transition range.

A third view comparing viscosities is given in Fig. 11, where the viscosities are plotted vs time for the three temperatures. This view shows that the other models fail to capture the full dynamic range of behaviors, especially at the lowest temperature. At 675 °C the empirical fit indicates that the viscosity has nearly reached its equilibrium value, as also

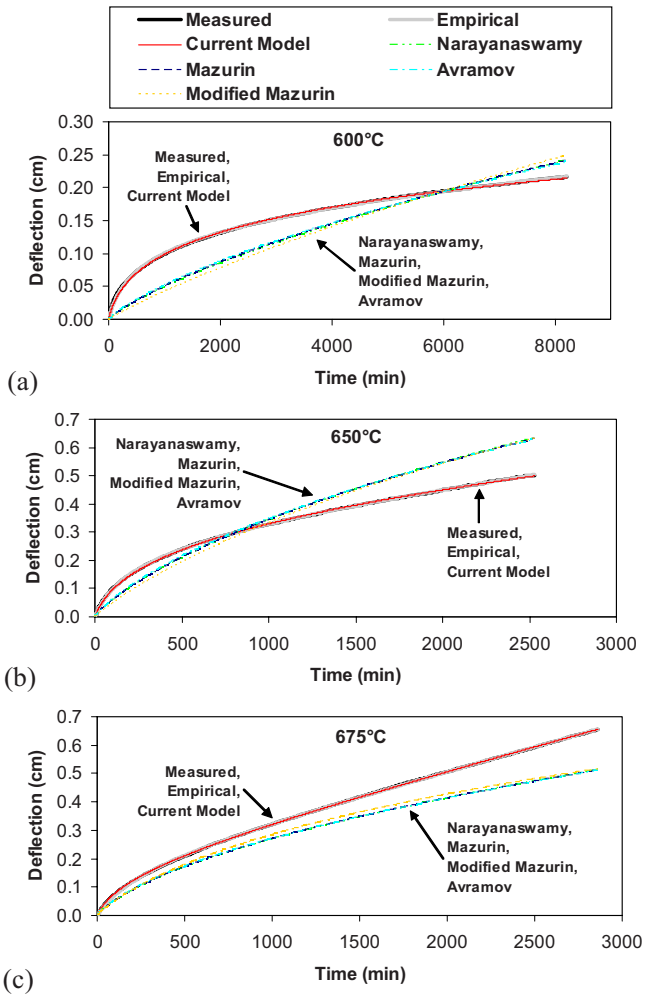

FIG. 9. (Color online) EAGLE XG™ deflection vs time measured and various model fits described in the text: (a) at 600 °C; (b) at 650 °C; and (c) at 675 °C.

shown by the current nonequilibrium viscosity model, but the other models still show a nonzero slope. These models are clearly missing an element of the rapid time-dependent evolution of viscosity. It is worth noting that at 600 °C the viscosity varies from an initial value of about $10^{14.3}$ to about $10^{15.9}$ Pa s, a factor of about 40 in viscosity, in about 5.7 days at 600 °C, and the viscosity has not reached its equilibrium value yet. This ratio of ending to starting viscosity is only about 5.5 at 675 °C from start to end of that measurement. The ratio would be higher in both cases if the glass had not relaxed somewhat during the heating toward the target temperature of the measurement.

VII. IMPACT OF FRAGILITY ON NONEQUILIBRIUM VISCOSITY

Recent work by Yue[61] has shown an intimate connection between isostructural viscosity and liquid fragility, m. Fragility is an equilibrium property defined as the slope of the $\log_{10}\eta_{eq}$ versus T_g/T curve at the glass transition temperature,[46,67–74]

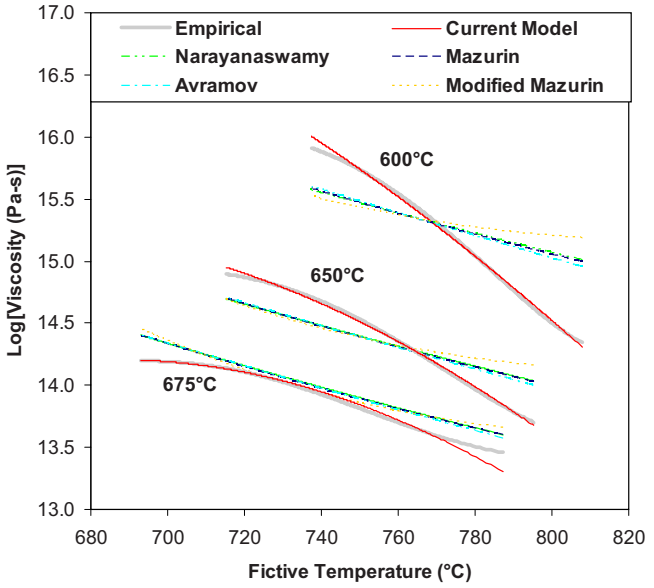

FIG. 10. (Color online) Empirical and model $\log_{10}\eta$ vs fictive temperature T_f for EAGLE XG™. The empirical (gray curves) and current model viscosities (red curves) are close together and have higher slope vs T_f than those of the other models, especially at 600 °C.

$$m \equiv \left.\frac{d\log_{10}\eta_{eq}}{d(T_g/T)}\right|_{T=T_g}, \tag{39}$$

where the glass transition temperature is defined as the temperature at which the equilibrium liquid viscosity is equal to 10^{12} Pa s. The work of Yue[61] is remarkable in that it shows how nonequilibrium viscosity is related to equilibrium viscosity parameters. In this section we extend Yue's analysis

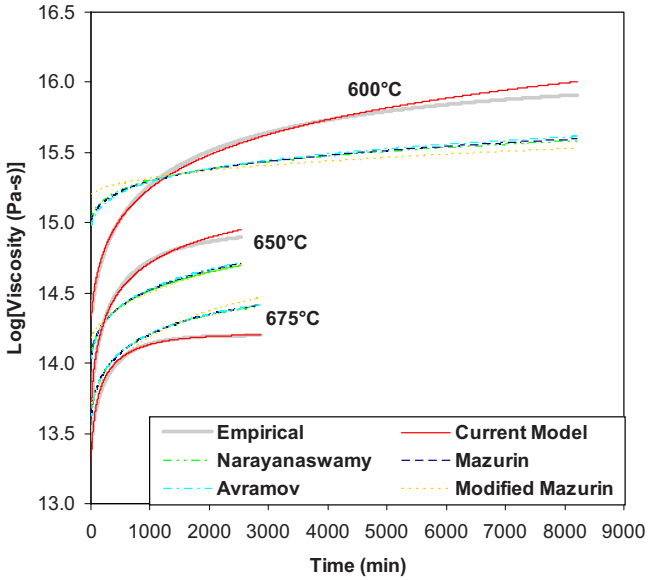

FIG. 11. (Color online) Empirical and model viscosities vs time for EAGLE XG™. The empirical (gray curves) and current model viscosities (red curves) are close together at each temperature and have a greater change in value over the time interval shown.

using enthalpy landscape calculations and our phenomenological viscosity model of Sec. IV.

As noted in Sec. II, the activation enthalpies in selenium are dominated by bond angle and torsion angle transitions with a nearly constant $\Delta H=1$ eV. This leads to a simplified form for the equilibrium transition rate,[26]

$$K(T) = \nu g(T)\exp\left(-\frac{\Delta H}{kT}\right) = \nu \exp\left(-\frac{\Delta H - kT \ln g(T)}{kT}\right), \tag{40}$$

where ν is the attempt frequency and $g(T)$ is the total number of accessible transition points at temperature T. Combining Eqs. (11), (39), and (40), fragility can be expressed as

$$m = -\frac{1}{\ln 10} - \frac{d \log_{10}[\nu g(T)\exp(-\Delta H/kT)]}{d(T_g/T)}, \tag{41}$$

which reduces to

$$m = -\frac{1}{\ln 10}\left(1 + \frac{d \ln g(T)}{d(T_g/T)}\right) + \frac{\Delta H}{kT_g \ln 10}. \tag{42}$$

Since we wish to isolate the impact of fragility on nonequilibrium viscosity, we will construct a series of landscapes based on our calculated landscape for selenium. These landscapes simulate hypothetical glass formers that are identical to selenium in every respect except with different values of fragility. In other words, we wish to adjust the fragility of the system while maintaining the same equilibrium enthalpy and volume vs temperature curves and also a constant glass transition temperature T_g. Equation (42) provides two possible terms for adjusting fragility. However, the first term in Eq. (42) must be held constant since the shape of the $\ln g(T)$ function has a direct impact on equilibrium enthalpy and volume scaling. This leaves only ΔH as a free parameter for adjusting fragility, but adjustment of ΔH also affects the glass transition temperature (since a greater enthalpy barrier would lead to a higher T_g). To maintain a constant glass transition temperature, the transition rate (or, inversely, the structural relaxation time) must be held constant at $T=T_g$. Hence,

$$K(T_g) = \nu \exp\left(-\frac{\Delta H - kT_g \ln g(T_g)}{kT_g}\right) \tag{43}$$

must be held constant while simultaneously adjusting ΔH to vary the fragility,

$$\Delta H \rightarrow \Delta H + \delta H. \tag{44}$$

This can be accomplished by adding a constant to $\ln g(T)$,

$$\ln g(T) \rightarrow \ln g(T) + \delta \ln g, \tag{45}$$

where δH and $\delta \ln g$ are chosen to obtain a constant Gibbs free energy barrier, $\Delta G=\Delta H-kT_g \ln g(T_g)$, at the glass transition temperature,

$$\delta H = kT_g \delta \ln g. \tag{46}$$

Equation (46) therefore provides a relation for adjusting fragility while preserving a constant glass transition temperature and without altering the enthalpy or volume curves of the supercooled liquid.

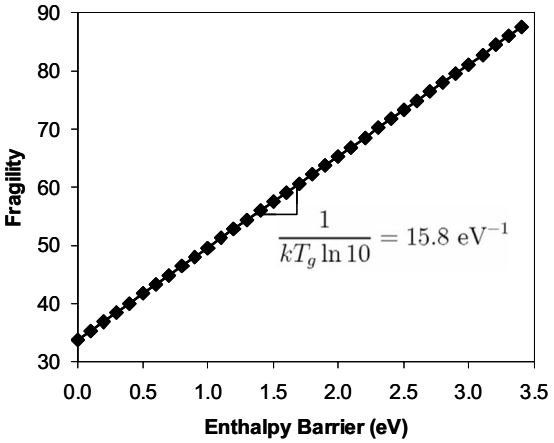

FIG. 12. Variation in fragility with enthalpy barrier.

Figure 12 plots the values of fragility obtained by adjusting the ΔH and $\ln g$ values of selenium as above. In the limit of $\Delta H \rightarrow 0$, Eq. (42) predicts a lower limit of fragility that is determined by the slope of the $\ln g(T)$ curve in Fig. 1. For an enthalpy landscape based on our model of selenium, this lower limit is $m=33.84$. (A lower fragility could be obtained with a flatter $\ln g(T)$ curve.) There is no theoretical upper limit to fragility,

$$\lim_{\Delta H \rightarrow \infty} m \rightarrow \infty. \tag{47}$$

As indicated in Eq. (42) and in Fig. 12, the slope of the m vs ΔH curve is governed solely by the glass transition temperature,

$$\frac{dm}{d\Delta H} = \frac{1}{kT_g \ln 10}. \tag{48}$$

Please note that ΔH is exactly the isostructural activation barrier in our nonequilibrium viscosity model of Sec. IV. Hence, the preceding analysis shows a direct linear relationship between ΔH and fragility.

Figure 13(a) plots the volume-temperature curves for three systems with identical glass transition temperature but different values of fragility. All three systems are cooled at a rate of 1 K/s. Figure 13(a) shows that increasing fragility leads to a sharper and more well-defined glass transition. With a higher fragility, the effective free energy barrier for structural relaxation increases more rapidly as the system is cooled through the glass transition. Above the glass transition dynamics are governed by entropic effects, i.e., the multitude of available transition states. Below the glass transition dynamics are governed by the enthalpic activation barriers. For a system with higher fragility there is a greater number of available transition points, but each having a higher activation enthalpy. Hence, systems with higher fragility have sharper crossover from entropy-dominated to enthalpy-dominated dynamics; this leads to a more sudden breakdown of ergodicity and a sharper glass transition. In a system with low fragility the transition from entropy-dominated to

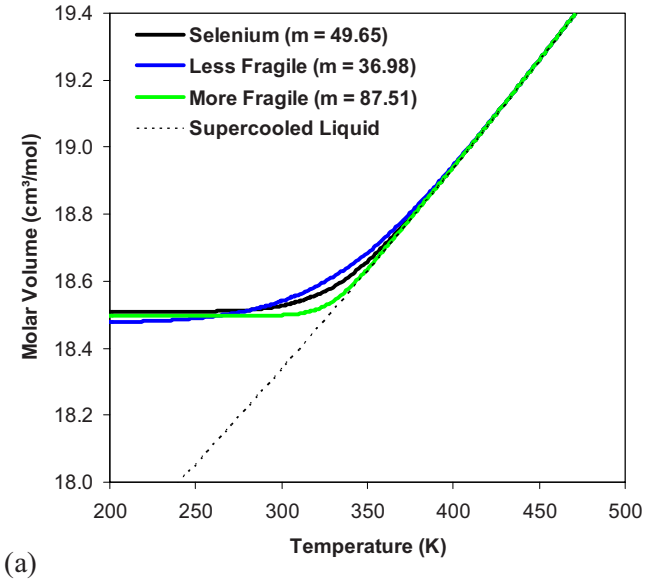

(a)

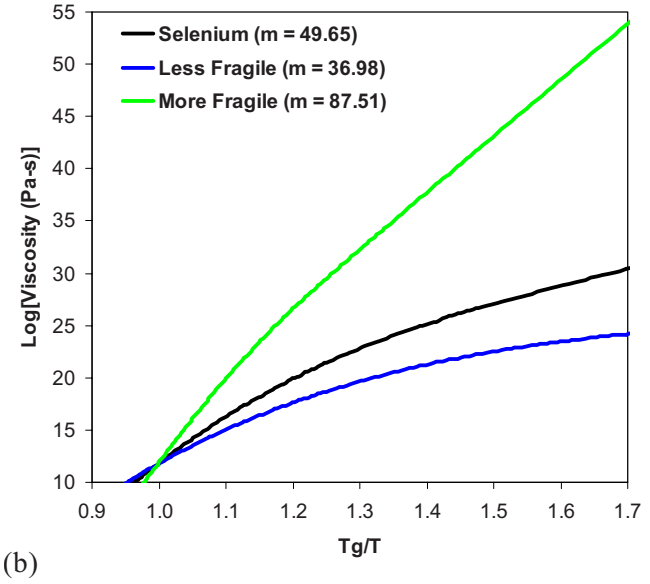

(b)

FIG. 13. (Color online) Computed (a) volume-temperature and (b) $\log_{10}\eta$ vs temperature curves for three glass-forming systems with different values of fragility. The cooling rate for all systems is 1 K/s. Increasing the fragility of the supercooled liquid results in a sharper glass transition and a higher nonequilibrium viscosity.

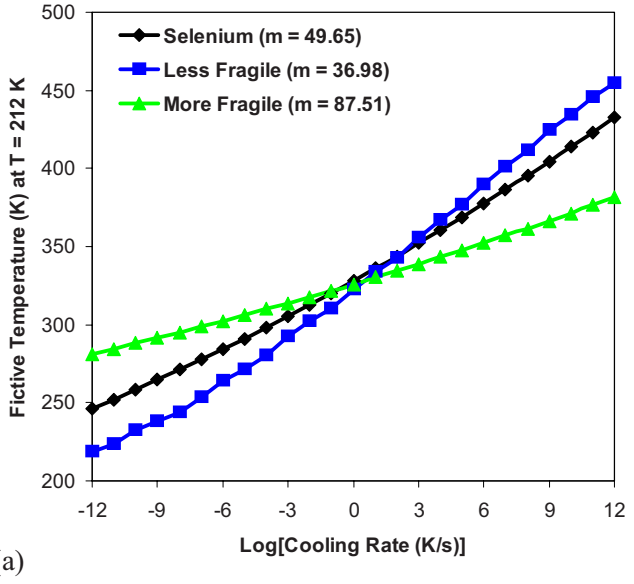

(a)

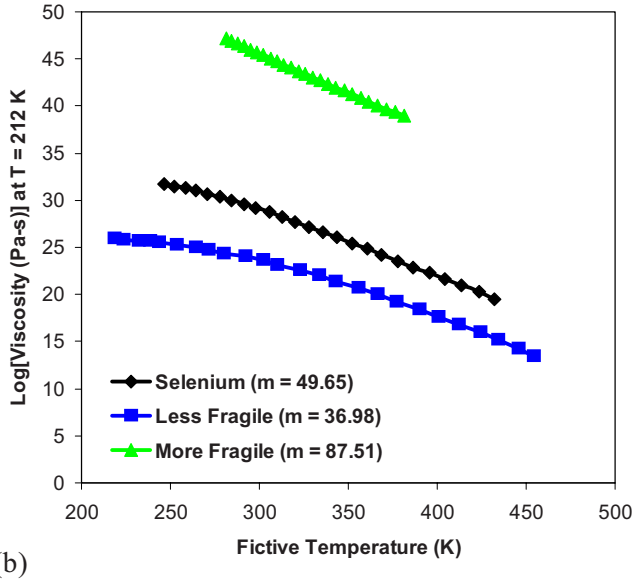

(b)

FIG. 14. (Color online) Variation in (a) fictive temperature with cooling rate and (b) nonequilibrium viscosity with fictive temperature for three glass-forming systems with different values of fragility.

enthalpy-dominated dynamics is blurred, leading to a more gradual loss of ergodicity and a broader glass transition range. The nonequilibrium viscosity curves for these three systems are plotted in Fig. 13(b). The steeper nonequilibrium viscosity curves for the more fragile systems are a direct result of the relationship between ΔH and m shown in Fig. 12.

Next we consider the impact of fragility on the cooling rate dependence of nonequilibrium viscosity. Figure 14(a) plots the scaling of fictive temperature with cooling rate for the three systems with different values of fragility. All three systems exhibit a linear dependence of fictive temperature with the logarithm of the cooling rate and have a common value of T_f at 1 K/s. However, a higher fragility leads to a shallower slope of the T_f vs cooling rate curve. This is a direct result of the more fragile systems having a sharper breakdown of ergodicity. Above the glass transition a more fragile system has a shorter relaxation time compared to a system with lower fragility (since the more fragile system has a greater entropic contribution to the dynamics). Hence, for the same cooling rate the more fragile system is able to trace the equilibrium liquid line more closely as the system approaches the glass transition. Below T_g the more fragile system has a longer relaxation time owing to the higher activation enthalpy, leading to a more sudden freezing of the fictive temperature. The result is that systems with higher fragility have a narrower range of available fictive temperatures compared to systems with lower fragility. (It is interesting to note that in the limit of infinite fragility only a

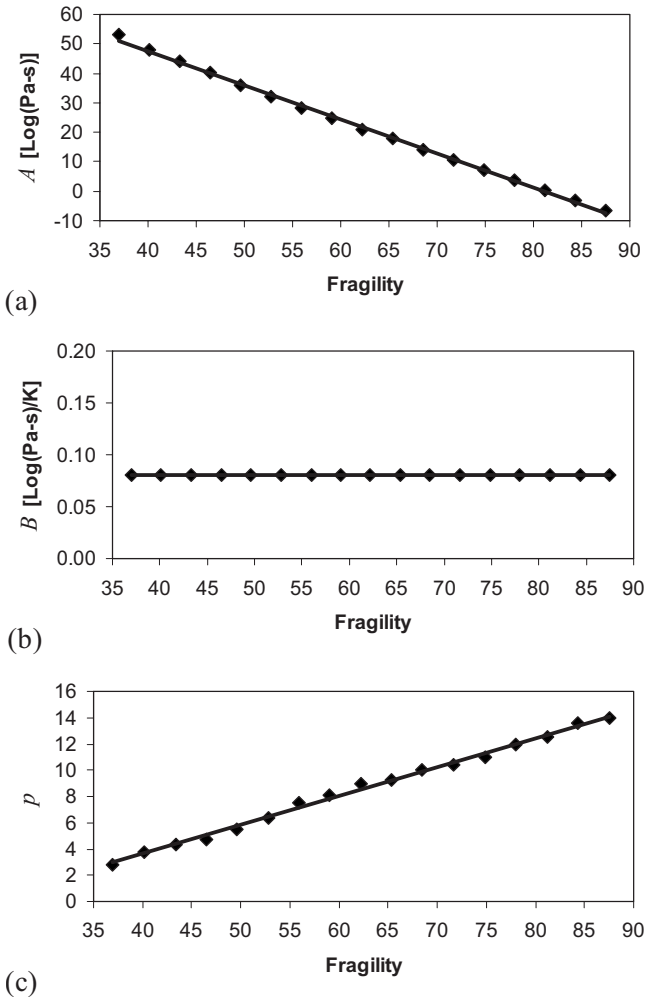

FIG. 15. Scaling of nonequilibrium viscosity parameters with fragility: (a) A from Eq. (27); (b) B from Eq. (27); and (c) p from Eq. (24). The ΔH parameter from Eq. (27) scales as in Fig. 12.

single fictive temperature is possible below the glass transition, viz., $T_f = T_g$. This limit corresponds to a discontinuous glass transition where there is a sudden and complete loss of ergodicity at T_g.) Figure 14(b) plots the corresponding nonequilibrium viscosity as a function of fictive temperature. All three systems exhibit a linear dependence of $\log_{10} \eta$ on fictive temperature except for the very slow cooling rates with low fragility (where there is insufficient departure from equilibrium).

With these calculations we can fit the nonequilibrium viscosity model of Sec. IV to the computed viscosity curves for all glasses. Figure 15(a) shows that the intercept parameter A of Eq. (27) decreases linearly with increasing fragility, whereas the fictive slope B is constant with respect to fragility. The constant B parameter follows directly from Fig. 14(b), which shows a constant slope for the $\log_{10} \eta$ vs T_f curves for all systems. In other words, $d \log_{10} \eta / dT_f$ is a constant in the isostructural regime, independent of fragility. To understand the linear decrease in A with fragility we must consider the physical meaning of this intercept parameter, which gives the $\log_{10} \eta$ value in the peculiar limit of $T_f \to 0$ and $T \to \infty$. Put another way, what is the viscosity of a system equilibrated in the zero temperature limit and then instantaneously upquenched to high temperature? This viscosity is lower for the more fragile systems since they have a greater number of available transition states. Finally, Fig. 15(c) shows that the power p in Eq. (24) increases linearly with fragility. This is expected from the work of Yue[61] and demonstrates the increasing sharpness of the glass transition with higher values of fragility. With these values of p and the fictive temperature evolution calculated from Eq. (14), Fig. 16 shows the scaling of the ergodicity parameter x with temperature; this clearly illustrates the sudden loss of ergodicity exhibited by highly fragile systems.

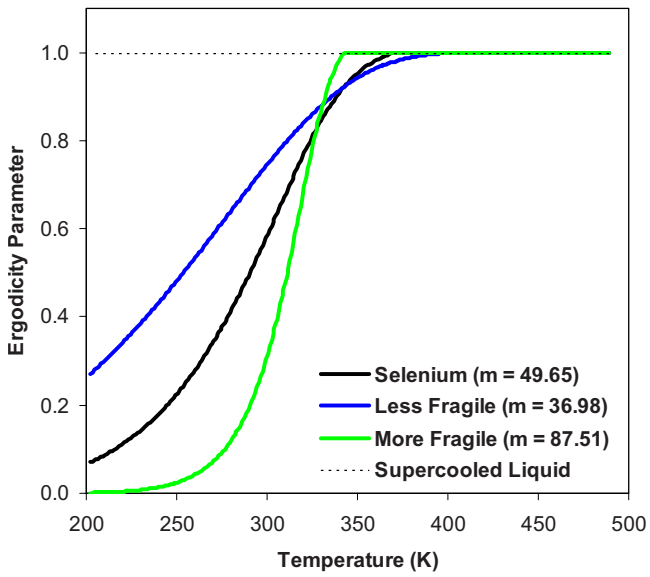

FIG. 16. (Color online) Evolution of the ergodicity parameter x from Eq. (24) for three glass-forming systems with different values of fragility. The cooling rate for all systems is 1 K/s. Increasing the fragility of the supercooled liquid results in a sharper loss of ergodicity (i.e., a sharper glass transition).

VIII. DISCUSSION

While the enthalpy landscape approach allows for calculation of glass viscosity on an arbitrary time scale, computation of enthalpy landscapes from first-principles requires the development of accurate interatomic potentials from *ab initio* simulations. Unfortunately, most potentials for oxide glass formers are empirical or semiempirical in nature and unsuitable for accurate landscape calculations. Given the long-range nature of forces, the development of new interatomic potentials for multicomponent industrial glasses is nontrivial.[11] To bypass this limitation, it is convenient to have a simple phenomenological model capturing the essential physics of glass viscosity with a small number of adjustable parameters. Our model of Sec. IV involves four such composition-dependent parameters:

(1) ΔH, the activation enthalpy for isostructural flow. At low temperatures the glass is effectively confined to a single basin in the enthalpy landscape. Shear flow requires escape from this basin, i.e., by overcoming the associated activation barrier ΔH. For selenium, ΔH is independent of thermal his-

tory: the super-Arrhenius scaling of selenium viscosity at equilibrium is due entirely to entropic effects, which produce a temperature-dependent Gibbs free energy barrier ΔG even with constant ΔH. Other studies have also shown that the temperature dependence of entropy plays the dominant role in governing the fragility of a variety of inorganic and organic liquids.[72,75–78] Hence, we believe that the thermal history dependence of ΔH is generally small, so the assumption of constant ΔH for a given composition is probably valid for most systems. However, the *composition dependence* of ΔH requires much further study. In Sec. VII we have shown a direct connection between fragility and ΔH for systems that differ only in their values of fragility (i.e., identical enthalpy- and volume-temperature curves of the supercooled liquid and identical glass transition temperature). It would be interesting to investigate this result in the laboratory; however, experimentally it is difficult to isolate the effect of fragility from changes in other properties.

(2) p, the exponent of the ergodicity parameter. While many models assume a discontinuous (i.e., perfectly sharp) glass transition, for any realistic system the glass transition is *continuous*.[30,33] In Sec. VII we have shown that the sharpness of the glass transition (as indicated by the value of p) scales proportionally with the liquid fragility. Higher values of fragility indicate a faster change in Gibbs free energy barrier ΔG as the system is cooled through the glass transition. Since ΔG at T_g is a constant for systems with identical glass transition temperature, a greater fragility indicates a lower ΔG above T_g and a higher ΔG below T_g. Hence, the more fragile system can trace the supercooled liquid curve more closely above T_g, but then it experiences a more sudden departure from equilibrium (i.e., a more sudden breakdown of ergodicity) immediately below T_g. The glass transition is discontinuous only in the (hypothetical) limit of infinite fragility or an infinitely fast quench. This connection between fragility and the sharpness of the glass transition has been noted previously by Angell based on experimental heat capacity curves.[74]

(3) B, the slope of viscosity with respect to fictive temperature in the isostructural regime. While the fictive temperature description of a glass is not rigorous (even when using a continuum of fictive temperatures[47]), it is a convenient parameter for modeling the thermal history dependence of glass properties such as viscosity. Two glasses of the same composition and at the same temperature-pressure conditions will exhibit different flow behaviors depending on their thermal histories. A faster cooled glass displays an earlier onset of the glass transition since there is less time for equilibration during cooling compared to a slowly cooled system. This leads to a higher fictive temperature for the faster cooled glass. Glasses with higher fictive temperature exhibit lower viscosity since they are trapped in a basin with a higher transition point entropy (i.e., more possible escape paths). In Sec. II we have shown that $\log_{10} \eta$ decreases linearly with fictive temperature in the isostructural regime (i.e., after complete breakdown of ergodicity). Unlike the other nonequilibrium viscosity parameters, the value of B is independent of liquid fragility.

(4) A, the intercept parameter. This parameter provides the constant offset for the nonequilibrium viscosity expression of Eq. (27). Physically, it corresponds to the viscosity of a glass in the limit of $T_f \to 0$ and $T \to \infty$. Implicit here is an assumption that the viscosity measurement is instantaneous [see Eq. (10)]. In other words, the glass is equilibrated at $T \to 0$, brought instantaneously to $T \to \infty$, and then its viscosity is measured in the next instant *before the glass has time to relax* at the high temperature. This, of course, is not a directly measurable quantity and must be obtained by extrapolation from available viscosity data. In Sec. VII we have shown that A decreases linearly with increasing fragility.

As demonstrated by our fits to the computed selenium data and the measured viscosity of EAGLE XG™ glass, the above parameters are sufficient to describe accurately the nonequilibrium viscosity over a wide range of temperatures and fictive temperatures. Further experimental and modeling work is required to characterize the detailed composition dependence of nonequilibrium viscosity. The use of hyperquenching would be particularly useful for experimentally accessing a wider range of thermal histories[73,79] and assessing the fictive temperature dependence of viscosity for different compositions. From a theoretical perspective, we believe there is much promise from use of topological modeling techniques to investigate the composition dependence of glass viscosity.[80–82]

IX. CONCLUSIONS

An accurate description of nonequilibrium viscosity is necessary for modeling and understanding the dynamics of glass. In this paper we adopted a truly multiscale approach, starting with rigorous enthalpy landscape calculations based on *ab initio* potentials for selenium. Based on these detailed results for selenium, we constructed a unified phenomenological model capable of representing viscosity in both the equilibrium and nonequilibrium regimes. By introducing an ergodicity parameter x, our model accounts for the continuous breakdown of ergodicity at the glass transition. Our current model provides a greatly improved fit of both the selenium calculations and the measurements of Corning EAGLE XG™ nonequilibrium viscosity. Finally we showed that fragility, an equilibrium liquid property, has a direct impact on the nonequilibrium viscosity of glass.

ACKNOWLEDGMENTS

The authors take great pleasure in acknowledging valuable discussions with Roger J. Loucks (Alfred University), Prabhat K. Gupta (Ohio State University), Yuanzheng Yue (Aalborg University), Roger J. Araujo, Adam J. Ellison, T. J. Kiczenski, Amy L. Rovelstad, Kamal Soni, and Pushkar Tandon (Corning Incorporated).

[1] E. D. Zanotto, Am. J. Phys. **66**, 392 (1998).
[2] H. Vogel, Phys. Z. **22**, 645 (1921).
[3] G. S. Fulcher, J. Am. Ceram. Soc. **8**, 339 (1925).
[4] G. Tammann, J. Soc. Glass Technol. **9**, 166 (1925).
[5] E. D. Zanotto and P. K. Gupta, Am. J. Phys. **67**, 260 (1999).
[6] G. W. Scherer, *Relaxation in Glass and Composites* (Wiley, New York, NY, 1986).
[7] A. K. Varshneya, *Fundamentals of Inorganic Glasses*, 2nd ed. (Society of Glass Technology, Sheffield, 2006).
[8] J. Zarzycki, *Glasses and the Vitreous State* (Cambridge University Press, Cambridge, 1990).
[9] D. R. Uhlmann and N. J. Kreidl, *Glass: Science and Technology* (Academic Press, New York, 1983).
[10] P. B. Macedo and A. Napolitano, J. Res. Natl. Bur. Stand., Sect. A **71**, 231 (1967).
[11] L. Wondraczek and J. C. Mauro, J. Eur. Ceram. Soc. **29**, 1227 (2009).
[12] J. C. Mauro and R. J. Loucks, Phys. Rev. B **76**, 174202 (2007).
[13] F. H. Stillinger, J. Phys. Chem. B **102**, 2807 (1998).
[14] T. F. Middleton and D. J. Wales, J. Chem. Phys. **118**, 4583 (2003).
[15] J. C. Mauro, R. J. Loucks, and J. Balakrishnan, J. Phys. Chem. B **110**, 5005 (2006).
[16] J. C. Mauro, R. J. Loucks, A. K. Varshneya, and P. K. Gupta, Sci. Model. Simul. **15**, 241 (2008).
[17] J. C. Mauro, S. S. Uzun, W. Bras, and S. Sen, Phys. Rev. Lett. **102**, 155506 (2009).
[18] J. C. Mauro and A. K. Varshneya, J. Am. Ceram. Soc. **89**, 1091 (2006).
[19] J. C. Mauro and A. K. Varshneya, Am. Ceram. Soc. Bull. **85**, 25 (2006).
[20] J. C. Mauro, R. J. Loucks, J. Balakrishnan, and A. K. Varshneya, J. Non-Cryst. Solids **353**, 1274 (2007).
[21] R. Zwanzig, *Nonequilibrium Statistical Mechanics* (Oxford University Press, Oxford, 2001).
[22] J. C. Mauro, R. J. Loucks, and J. Balakrishnan, J. Phys. Chem. A **109**, 9578 (2005).
[23] G. T. Barkema and N. Mousseau, Comput. Mater. Sci. **20**, 285 (2001).
[24] N. Mousseau and G. T. Barkema, Phys. Rev. B **61**, 1898 (2000).
[25] J. C. Mauro, R. J. Loucks, J. Balakrishnan, and S. Raghavan, J. Chem. Phys. **126**, 194103 (2007).
[26] J. C. Mauro, R. J. Loucks, and P. K. Gupta, J. Phys. Chem. A **111**, 7957 (2007).
[27] A. N. Sreeram, A. K. Varshneya, and D. R. Swiler, J. Non-Cryst. Solids **128**, 294 (1991).
[28] U. Senapati and A. K. Varshneya, J. Non-Cryst. Solids **197**, 210 (1996).
[29] P. K. Gupta and J. C. Mauro, J. Chem. Phys. **126**, 224504 (2007).
[30] J. C. Mauro, P. K. Gupta, and R. J. Loucks, J. Chem. Phys. **126**, 184511 (2007).
[31] P. K. Gupta and J. C. Mauro, J. Chem. Phys. **129**, 067101 (2008).
[32] P. K. Gupta and J. C. Mauro, J. Non-Cryst. Solids **355**, 595 (2009).
[33] J. C. Mauro, P. K. Gupta, R. J. Loucks, and A. K. Varshneya, J. Non-Cryst. Solids **355**, 600 (2009).
[34] F. H. Stillinger and T. A. Weber, Phys. Rev. A **25**, 978 (1982).
[35] F. H. Stillinger and T. A. Weber, Phys. Rev. A **28**, 2408 (1983).
[36] F. H. Stillinger, J. Chem. Phys. **88**, 7818 (1988).
[37] P. G. Debenedetti, F. H. Stillinger, T. M. Truskett, and C. J. Roberts, J. Phys. Chem. B **103**, 7390 (1999).
[38] P. G. Debenedetti and F. H. Stillinger, Nature (London) **410**, 259 (2001).
[39] F. H. Stillinger and P. G. Debenedetti, J. Chem. Phys. **116**, 3353 (2002).
[40] J. C. Mauro and A. K. Varshneya, Phys. Rev. B **71**, 214105 (2005).
[41] C. Møller and M. S. Plesset, Phys. Rev. **46**, 618 (1934).
[42] A. K. Wilson, D. E. Woon, K. A. Peterson, and T. H. Dunning, Jr., J. Chem. Phys. **110**, 7667 (1999).
[43] J. C. Mauro, R. J. Loucks, J. Balakrishnan, and A. K. Varshneya, J. Non-Cryst. Solids **353**, 1268 (2007).
[44] S. Sastry, P. G. Debenedetti, and F. H. Stillinger, Nature (London) **393**, 554 (1998).
[45] T. B. Schrøder, S. Sastry, J. C. Dyre, and S. C. Glotzer, J. Chem. Phys. **112**, 9834 (2000).
[46] C. A. Angell, J. Non-Cryst. Solids **73**, 1 (1985).
[47] J. C. Mauro, R. J. Loucks, and P. K. Gupta, J. Am. Ceram. Soc. **92**, 75 (2009).
[48] J. C. Mauro and R. J. Loucks, J. Non-Cryst. Solids **355**, 676 (2009).
[49] O. S. Narayanaswamy, J. Am. Ceram. Soc. **54**, 491 (1971).
[50] G. Adam and J. H. Gibbs, J. Chem. Phys. **43**, 139 (1965).
[51] W. Kauzmann, Chem. Rev. (Washington, D.C.) **43**, 219 (1948).
[52] F. H. Stillinger, P. G. Debenedetti, and T. M. Truskett, J. Phys. Chem. B **105**, 11809 (2001).
[53] D. Huang, S. L. Simon, and G. B. McKenna, J. Chem. Phys. **119**, 3590 (2003).
[54] S. L. Simon and G. B. McKenna, J. Non-Cryst. Solids **355**, 672 (2009).
[55] J. C. Mauro, Y. Z. Yue, A. J. Ellison, P. K. Gupta, and D. C. Allan (unpublished).
[56] O. V. Mazurin, V. P. Kluyev, and S. V. Stolyar, Glastech. Ber. **56K**, 1148 (1983).
[57] O. V. Mazurin, *Steklovanie (Glass Transition)* (Nauka, Leningrad, 1986).
[58] A. I. Priven, Glass Phys. Chem. **27**, 527 (2001).
[59] I. Avramov, J. Chem. Phys. **95**, 4439 (1991).
[60] I. Avramov and A. Milchev, J. Non-Cryst. Solids **104**, 253 (1988).
[61] Y. Z. Yue, J. Non-Cryst. Solids **355**, 737 (2009).
[62] ASTM C1350-96 (reapproved 2003), Standard Test Method for Measurement of Viscosity of Glass Between Softening Point and Annealing Range (approximately 10^8 Pa s to approximately 10^{13} Pa s) by Beam Bending (Metric).
[63] L. D. Landau and E. M. Lifshitz, *Theory of Elasticity*, 3rd ed. (Butterworth-Heinemann, Boston, 1986), p. 81.
[64] Y. Z. Yue, J. D. Christiansen, and S. L. Jensen, Chem. Phys. Lett. **357**, 20 (2002).
[65] D. C. Allan and M. Potuzak, Proceedings of the 15th International Display Workshops, Society for Information Display (Niigata, Japan, 2008), pp. 1653–1656.
[66] W. H. Press, S. A. Teukolsky, W. T. Vetterling, and B. P. Flannery, *Numerical Recipes*, The Art of Scientific Computing, 3rd ed. (Cambridge University Press, New York, NY, 2007).
[67] C. A. Angell, J. Non-Cryst. Solids **102**, 205 (1988).
[68] C. A. Angell, J. Non-Cryst. Solids **131-133**, 13 (1991).
[69] C. A. Angell, K. L. Ngai, G. B. McKenna, P. F. McMillan, and S.

W. Martin, J. Appl. Phys. **88**, 3113 (2000).
[70] R. Böhmer and C. A. Angell, Phys. Rev. B **45**, 10091 (1992).
[71] J. C. Mauro and R. J. Loucks, Phys. Rev. E **78**, 021502 (2008).
[72] P. K. Gupta and J. C. Mauro, Phys. Rev. E **78**, 062501 (2008).
[73] L. Hornbøll and Y. Z. Yue, J. Non-Cryst. Solids **354**, 350 (2008).
[74] C. A. Angell, Chem. Rev. (Washington, D.C.) **102**, 2627 (2002).
[75] U. Mohanty, N. Craig, and J. T. Fourkas, J. Chem. Phys. **114**, 10577 (2001).
[76] D. Cangialosi, A. Alegría, and J. Colmenero, J. Chem. Phys. **124**, 024906 (2006).
[77] L.-M. Wang, C. A. Angell, and R. Richert, J. Chem. Phys. **125**, 074505 (2006).
[78] V. Lubchenko and P. G. Wolynes, J. Chem. Phys. **119**, 9088 (2003).
[79] Y. Z. Yue, Phys. Chem. Glasses **46**, 354 (2005).
[80] P. K. Gupta and J. C. Mauro, J. Chem. Phys. **130**, 094503 (2009).
[81] M. Micoulaut, Am. Mineral. **93**, 1732 (2008).
[82] M. Micoulaut and J. C. Phillips, J. Non-Cryst. Solids **353**, 1732 (2007).